TI Designs
RF Sampling S-Band Radar Receiver

TEXAS INSTRUMENTS

Design Overview

A direct RF sampling receiver approach to a radar system operating in S-band is demonstrated using the ADC32RF45, 3-GSPS, 14-bit, dual channel analog-to-digital converter (ADC). RF sampling reduces the complexity of a system by removing downconversion stages and using a high sampling rate enables wider signal bandwidths. The approach is demonstrated by building a receiver based on the ASR-11 air traffic control radar specifications.

Design Resources

|	
TIDA-00814	Design Folder
ADC32RF45	Product Folder
TSW14J56	Product Folder
LMK04828	Product Folder

TI E2E™ Community

ASK Our E2E Experts

Design Features

- S-Band Radar Reference Design
- Example Lineup Analysis With RF Sampling ADC
- Measurements Verify Calculated Performance
- Radar Specific Measurements With Detection Scheme
- Supports Greater Than 1-GHz Instantaneous Signal Bandwidth

Featured Applications

- Air Traffic Control Radar
- Weather Radar
- Military Radar
- RF Sampling Communications Systems
- Radar-Based Level Sensing
- Radar-Based Distance Measurement

Copyright © 2016, Texas Instruments Incorporated
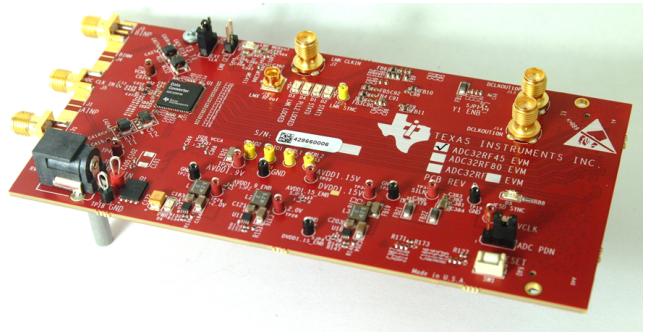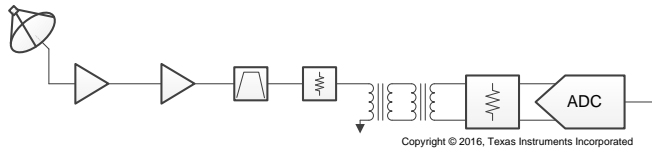
An IMPORTANT NOTICE at the end of this TI reference design addresses authorized use, intellectual property matters and other important disclaimers and information.

1   Key System Specifications

Table 1. Radar Design Specifications

PARAMETER	SPECIFICATION	DETAILS
Target cross section	1 m^2	—
Range	0.5 km to 100 km	—
RF carrier frequency	2.8 GHz	—
Transmit power	12.5 kW 25.0 kW	0.5 km to 30 km 29 km to 100 km
Pulse type	Linear frequency modulation (LFM)	—
Pulse length	1 µs 89 µs	0.5 km to 30 km 29 km to 100 km
Pulse bandwidth	100 MHz	—
Antenna gain	34 dBi	ASR-11 Antenna [1] [2]
Detection probability (P_D)	0.8	For a single pulse
False alarm probability (P_{FA})	10^{-6}	For a single pulse

2 System Description

The TIDA-00814 reference design shows the use of direct radio frequency (RF) sampling in radar receiver applications. The focus of this design application is radar operating in S-band (2 GHz to 4 GHz), where direct RF sampling is possible using the ADC32RF45, 3-Gsps, 14-bit, dual channel analog-to-digital converter (ADC). The 3.3-GHz input bandwidth (BW) of the ADC32RF45 can be stretched to support 4 GHz with some allowable attenuation. This reference design has been designed to operate as an air traffic control radar (airport surveillance radar) similar to the ASR-11 radar currently in operation at the time of this writing [1] [2]. Figure 1 shows the use case where the radar can detect planes from 500 m to 100 km. The design uses two different pulses: one to detect targets near the airport and one to detect targets far from the airport. The range of these pulses is defined as 0.5 km to 30 km and 29 km to 100 km, respectively.
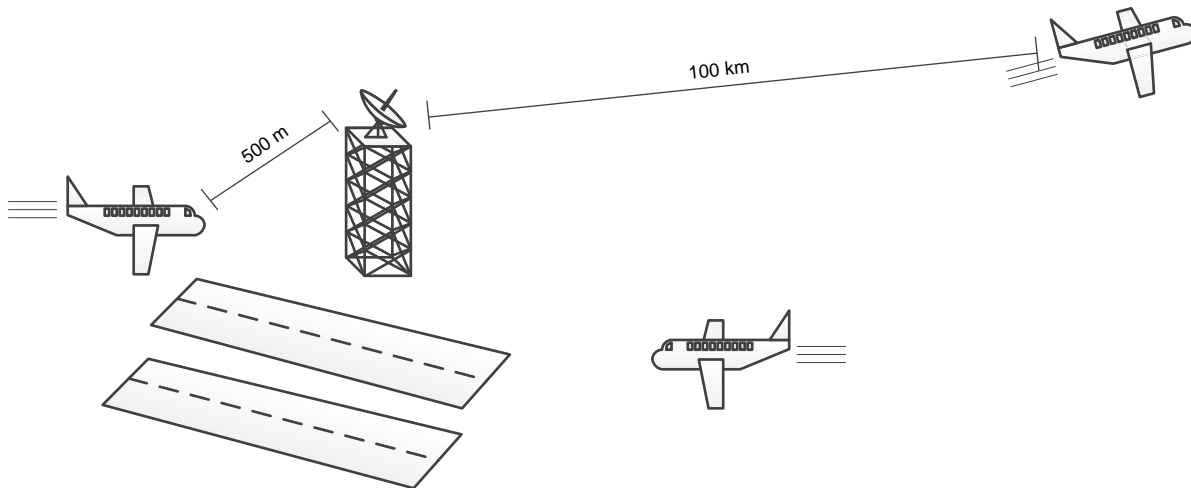

Figure 1. Airport Air Traffic Control Radar Use Case

The receiver only requires using amplifiers, filters, transformers (or baluns), and the RF sampling ADC32RF45 device. This architecture does not require analog mixing stages or local oscillators (LO), thereby reducing the overall component count and size of the solution.

The performance of the receiver is analyzed and then verified through measurement. A matched-quadrature filter detector is used with a simulated radar return signal generated by a digital-to-analog converter (DAC). Gain or phase equalization is not used in the measurement; however, the addition of equalization may increase the performance of the receiver. Note that the ASR-11 specifications have been modified to fit components that were readily available in the lab for testing.

3   Block Diagram

Figure 2 shows the block diagram for the TIDA-00814 reference design. The most obvious benefit of the RF sampling architecture is the low number of components required when comparing to a traditional heterodyne architecture. The main components that this design uses are two amplifiers, a bandpass filter, an attenuator, transformers, and an ADC32RF45 device. Section 4.6 describes these components in more detail.

Copyright © 2016, Texas Instruments Incorporated
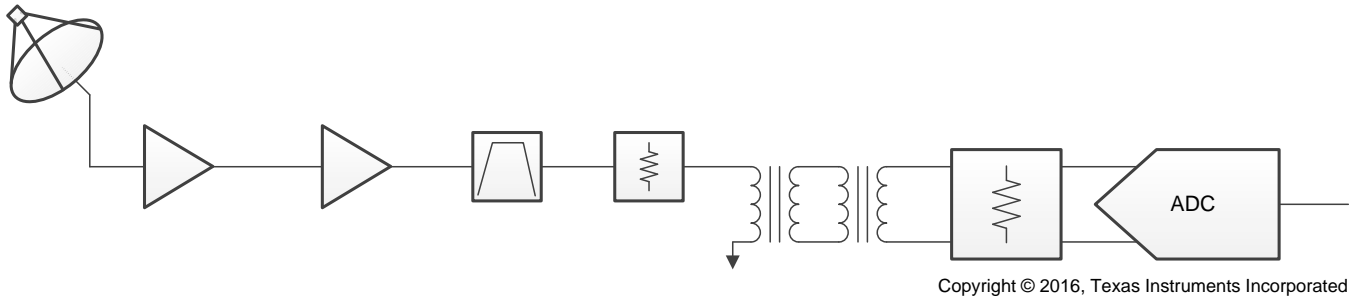
Figure 2. TIDA-00814 Block Diagram

## 3.1   Highlighted Products

3.1.1   ADC32RF45

The essential component for the direct RF sampling radar in the TIDA-00814 design is the ADC32RF45, which is a 14-bit, 3-GSPS ADC. The ADCs low noise floor and high bandwidth enable use of the ADC for direct RF sampling through L-band and S-band frequency ranges. The ADC has a number of features to improve direct RF sampling performance and simplify radar architectures.

The ADC32RF45 has a multiband digital-down conversion (DDC) block for each ADC channel. Two separate frequency bands can be downconverted simultaneously from the captured signal at the ADC output for each ADC channel. This feature enables downconversion of up to four frequencies for a single ADC32RF45 device. The DDC block allows offloading of digital mixing and decimation from the field programmable gate array (FPGA) while also reducing total data throughput and power consumption of the interface. Additionally, if the designer uses a single down-converter per ADC channel, the designer can hop the mixing frequency by switching between three independent NCOs per channel. The NCO that is not selected during this time continues to run so that hopping back to that frequency maintains the phase coherency.

Figure 3 shows the block diagram for the ADC32RF45. The diagram shows various DDCs as well as the DDC bypass, which can be used to enable the full data rate.
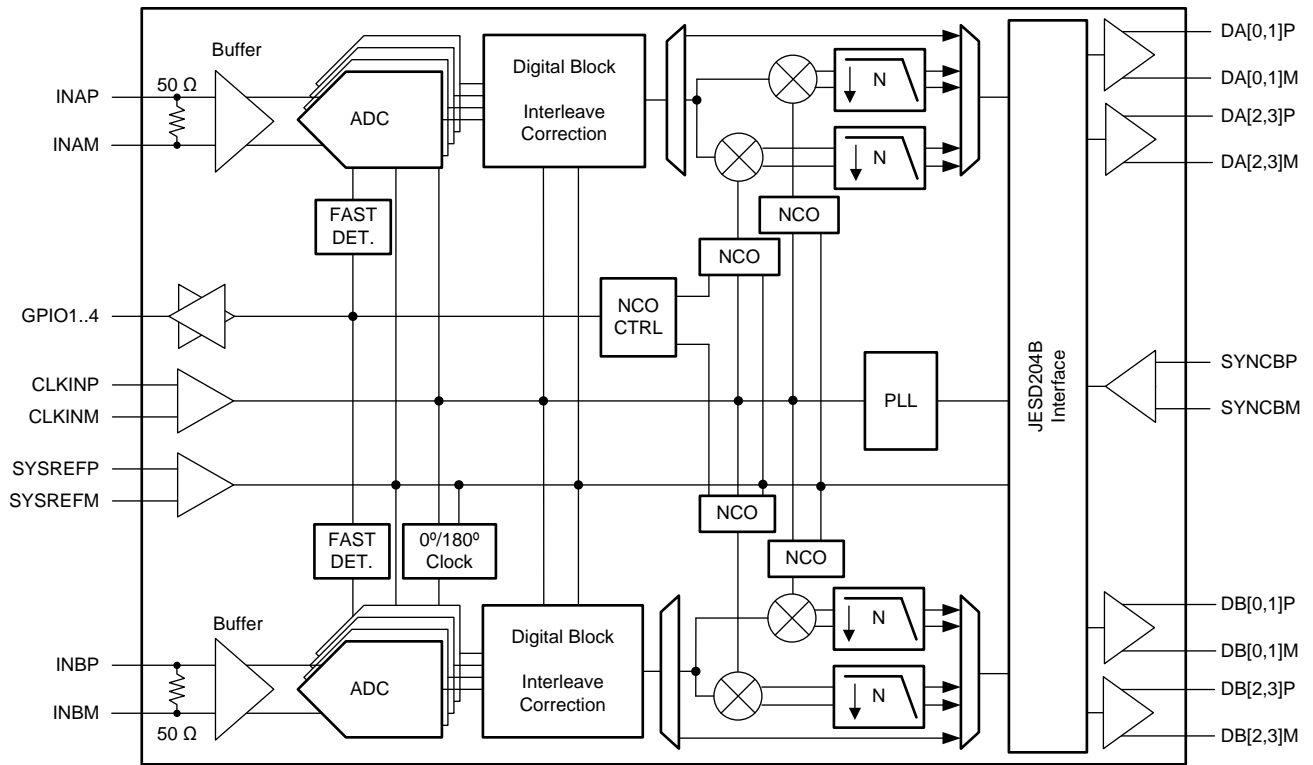
Copyright © 2016, Texas Instruments Incorporated

Figure 3. ADC32RF45 Block Diagram

# 4 System Design Theory

4.1 Radar Signals

The design uses two radar signals based on two ranges to limit the average transmit power. For targets from 500 m to 30 km, a linear frequency modulated (LFM) pulse with a period of 1 µs and transmit power of 12.5 kW is used. For targets from 29 km to 100 km, an LFM pulse with a period of 89 µs and transmit power of 25 kW is used. The longer pulse length, in addition to a higher transmit power, increases the energy of the return signal. The ranges overlap to ensure that there are no dead spots. Table 2 shows the two ranges and their respective signal types and pulse lengths.

Table 2. Summary of Radar Transmit Signals for Defined Ranges

RANGE	PULSE TYPE	TRANSMIT POWER	PULSE LENGTH	TRANSMIT ENERGY	CENTER FREQUENCY	SIGNAL BANDWIDTH
500 m to 30 km	LFM	12.5 kW	1 µs	0.0125 J	2.8 GHz	100 MHz
29 km to 100 km	LFM	25 kW	89 µs	2.23 J	2.8 GHz	100 MHz

4.2 Transmit and Dwell Times

Figure 4 shows the transmit time, dead time, dwell times, and associated ranges for the two radar pulses. The minimum distance for each range sets the maximum pulse width. The gray areas in the figure indicate the dead time during the switch from transmission to receive operation. The propagation delays are based on the speed of light in free space, which is 3.33 ns/m.
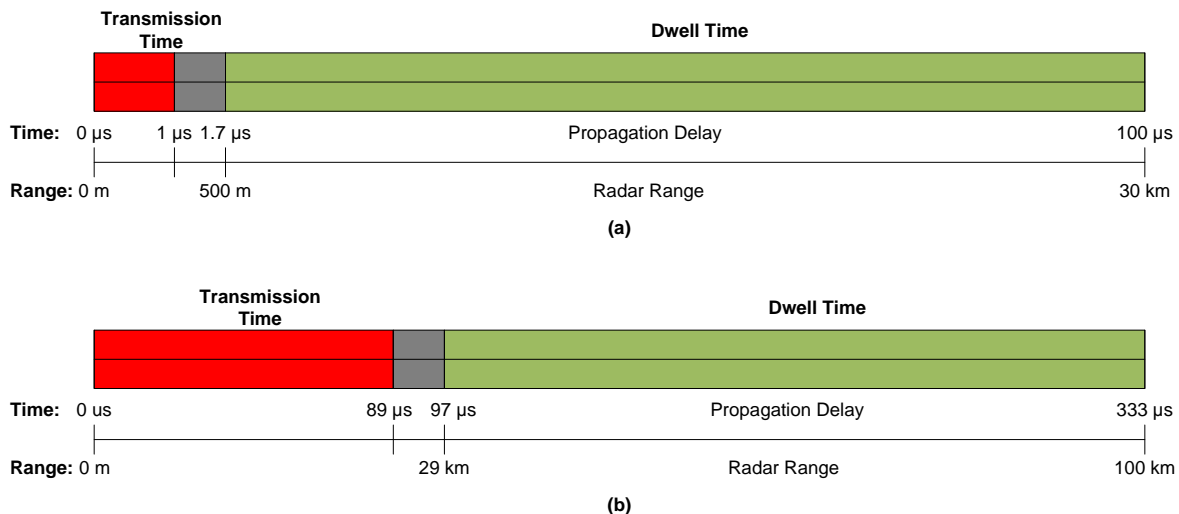
Figure 4. Transmission, Dwell Times, and Ranges for Near (a) and Far (b) Targets

4.3 Radar Range and Receive Signal

The common radar equation can be used to find the total attenuation of the signal to the target and back by using the required range, frequency, transmission power, and antenna gain. Equation 1 shows the basic form of the radar equation:

$$P_r = \frac{P_t G_t}{4\pi R^2} \times \frac{\sigma}{4\pi R^2} \times A_e$$

(1)

If the designer assumes that the transmit and receive antenna are the same, then the designer can replace the effective aperture (A_e) by using the relationship between transmit gain and receive effective aperture, as in Equation 2:

$$A_e = \frac{G_t \times \lambda^2}{4\pi}$$

(2)

$$P_r = \frac{P_t G_t^2 \times \sigma \times \lambda^2}{(4\pi)^3 \times R^4}$$

(3)

Equation 4 calculates the propagation attenuation, α, where α is defined as a gain and can be defined as P_r / P_t. This propagation attenuation provides a relationship between the receive power and transmit power independent of the transmit power.

$$\alpha = \frac{P_r}{P_t} = \frac{G_t^2 \times \sigma \times \lambda^2}{(4\pi)^3 \times R^4}$$

(4)

The returned power of the return pulse is then equal to the following calculation in Equation 5:

$$P_r = \alpha \times P_t$$

(5)

Table 3 shows a summary of the minimum and maximum propagation attenuation (α) and received power for the defined radar signals and ranges.

Table 3. Propagation Attenuation and Return Signal Power Versus Range

RANGE	P_t	MAX α	MIN α	MAX P_r	MIN P_r
500 m to 30 km	12.5 kW	−92.3 dB	−163.5 dB	−21.4 dBm	−92.5 dBm
29 km to 100 km	25 kW	−162.9 dB	−184.4 dB	−88.9 dBm	−110.4 dBm

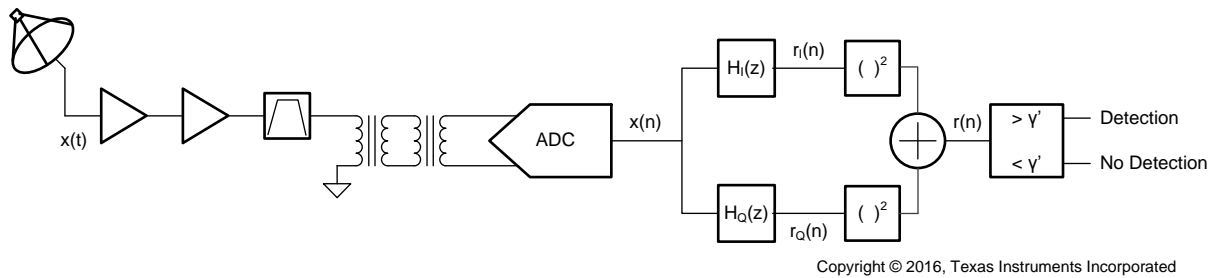Similarly, the return power can be calculated across the full radar range, as Figure 5 shows.
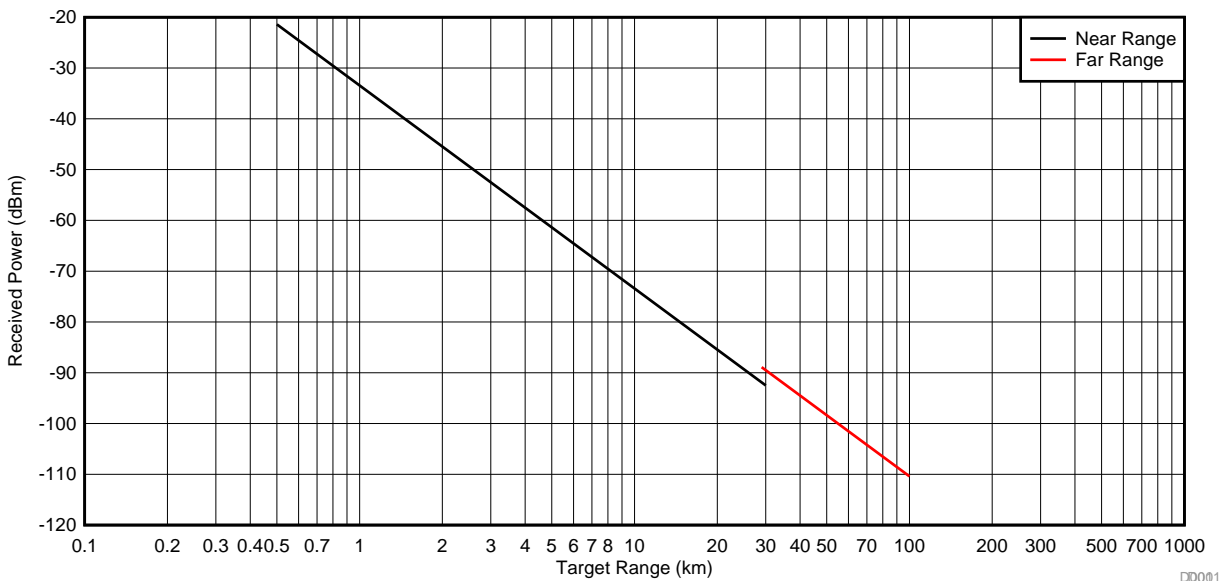
Figure 5. Received Power vs Radar Range

4.4 Receiver Performance

After calculating the received power at the farthest distance for each signal, the designer can determine the required noise performance of the receiver. Figure 6 shows a block diagram of the radar receiver.

Figure 6. Radar Receiver Block Diagram

The signal received at the antenna is x(t) and the sampled signal is x(n). The detection scheme uses a quadrature matched filter, where the filters $H_I(z)$ and $H_Q(z)$ are in-phase and quadrature-phase matched filters of transmitted LFM signal, respectively. Each filter has a length of M and amplitude of the square root of M. The resulting complex filter has a constant envelope. The output of the filters are defined as $r_I(n)$ and $r_Q(n)$. The sum of squares of $r_I(n)$ and $r_Q(n)$, called r(n), is used as the decision signal and compared against a fixed threshold, γ', to determine whether a target is present. The following Equation 6, Equation 7, and Equation 8 show these relationships:

$$r_I\left(n\right) = \frac{1}{\sqrt{M}} \times \sum_{k=0}^{M-1} h_I(k)\, \chi\left(n-k\right)$$

(6)

$$r_Q\left(n\right) = \frac{1}{\sqrt{M}} \times \sum_{k=0}^{M-1} h_Q\left(k\right) \chi\left(n-k\right)$$

(7)

$$r\left(n\right) = r_I\left(n\right)^2 + r_Q\left(n\right)^2$$

(8)

The specification requires the probability of detecting detection (P_D) for a target at 100 km away from the radar for a single pulse to beas 0.8 and a false alarm probability (P_{FA}) of 10^{-6}. The envelope detector, defined as r(n), has a central chi-squared distribution when no target is present and a non-central, chi-squared distribution when a target is present. A look-up table can be used to find the energy-to-noise ratio (ENR) that is required to meet the P_D and P_{FA} specifications, which has been found as 35.5 (15.5 dB) for this system [3]. The ENR, defined below in the following Equation 9 as λ, can then be used to find the required noise spectral density of the system.

$$\lambda = \frac{M \times A^2}{2 \times \sigma^2}$$

(9)

ENR is a function of the received signal amplitude and the noise variance. Rewriting the ENR in terms of the analog, received signal energy and solving for the noise variance results in Equation 10:

$$\lambda = \frac{P_r \times T_P}{\sigma_A^2}$$

$$\sigma_A^2 = \frac{P_r \times T_P}{\lambda}$$

where

- σ_A^2 represents the required input-referred noise power of the receiver.

(10)

σ_A^2 can then be calculated in terms of dBm/Hz (see Equation 11). Table 4 summarizes the results for the maximum ranges for each signal (near and far) and the required noise figure (NF) is calculated assuming −174 dBm/Hz as the input signal noise spectral density.

$$P_N\left[\frac{dBm}{Hz}\right] = 10\,\log_{10} \times \frac{\sigma^2}{0.001} = P_r\left[\frac{dBm}{Hz}\right] + 10\,\log_{10} \times T_P - ENR[dB]$$

(11)

Table 4. Required Input Referred Noise Floor and Noise Figure for Worst-Case Ranges

RANGE	P_t	T_P	P_r [dBm]	REQUIRED P_N [dBm/Hz]	MAXIMUM NF [dB]
30 km	12.5 kW	1 µs	−92.5 dBm	−168	6
100 km	25 kW	89 µs	−110.4 dBm	−166.4	7.6

Because the 30-km range has a stricter noise figure requirement, this specification sets the noise figure requirement for the receiver.

4.5 Detection Threshold

Find the detection rule based on the probability distribution functions of r(n) for a target being present and a target not being present at each time point, n, which is defined as events H_1 and H_0, respectively. The decision rule is compactly defined as shown in Equation 12:

$$r\left(n\right) \underset{H_0}{\overset{H_1}{\underset{<}{\gtrless}}} \gamma'$$

where

- The threshold, γ', is defined by a likelihood ratio test, using the Neyman-Pearson lemma [3]   (12)

The resulting false alarm probability and detection probability for a single pulse have been defined in the following Equation 13 and Equation 14 in terms of the threshold, γ'.

$$P_{FA} = P_r\left\{r\left(n\right) > \gamma';H_0\right\} = e^{-\frac{\gamma'}{\sigma^2}}$$

(13)

$$P_D = P_r\left\{r\left(n\right) > \gamma';H_1\right\} = Q_{x_2'^2(\lambda)}\times\left(\frac{2\times\gamma'}{\sigma^2}\right)$$

(14)

The noise variance for the threshold calculation can be determined as the variance of the output of one of the I or Q matched filters given in Equation 6 and Equation 7 when no target is present. Equation 15 and Equation 16 provide the distributions for $r_I(n)$ and $r_Q(n)$ for reference:

$$r_I(n) \sim \begin{cases} N\left(0, \dfrac{\sigma^2}{2}\right) \text{ given } H_0 \\ N\left(\dfrac{\sqrt{MA}}{2}, \dfrac{\sigma^2}{2}\right) \text{ given } H_1 \end{cases}$$

(15)

$$r_Q(n) \sim \begin{cases} N\left(0, \dfrac{\sigma^2}{2}\right) \text{ given } H_0 \\ N\left(\dfrac{\sqrt{MA}}{2}, \dfrac{\sigma^2}{2}\right) \text{ given } H_1 \end{cases}$$

(16)

Equation 17 calculates the expected value of r(n) when a target is present, which can then be used to find the amplitude of the received signal. The approximation assumes that the signal energy is much greater than the noise variance.

$$E\left[r(n) \mid H_1\right] \cong \frac{MA^2}{4}$$

(17)

4.6   Receiver Design

Based on the results in the previous subsection, a receiver lineup has been designed and measured in the lab to meet the required noise figure. Note that the third order intercept point (IIP3) has been ignored when generating the receiver requirements; however, this value has been calculated in the following Figure 7 for reference.

G = 16.44 dB   G = 16.44 dB   G = −0.34 dB   G = −3 dB   G = −1.2 dB   G = −1.85 dB   G = 0 dB   **Totals:**
NF = 3.0 dB   NF = 3.0 dB   NF = 0.34 dB   NF = 3 dB   NF = 1.2 dB   NF = 1.85 dB   NF = 25.6 dB   G = 26.49 dB
IIP3 = 25.6 dBm IIP3 = 25.6 dBm   IIP3 = 29 dBm   NF = 4.53 dB
                                                                                                           IIP3 = 1.64 dBm

Copyright © 2016, Texas Instruments Incorporated
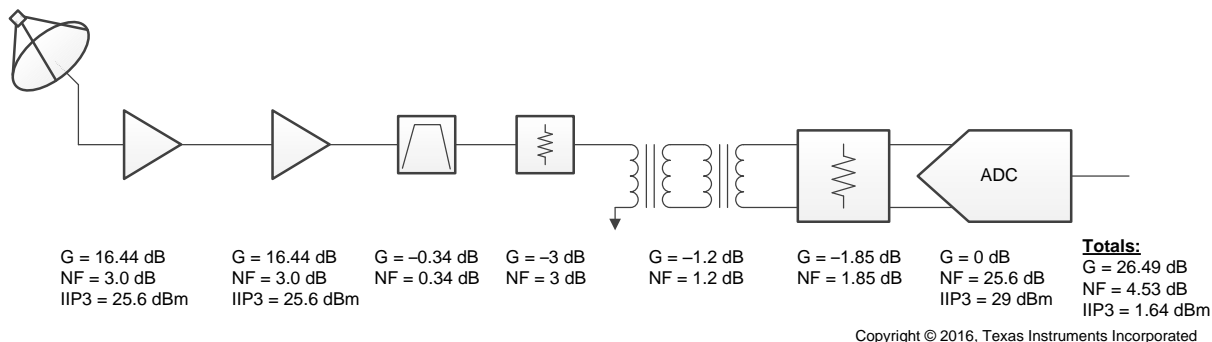
Figure 7. Lineup Analysis for Receiver Used in Lab Measurements

The designed receiver consists of two RF amplifiers, an attenuator, a bandpass filter, two transformers, and an ADC32RF45 device. The amplifiers are Mini-Circuits ZRL-3500+ amplifiers and were readily available in the lab. The bandpass filter is a tunable filter with a bandwidth of approximately 100 MHz that removes wideband noise and interferers from the antenna and amplifiers. The attenuator is placed at the input to the ADC32RF45 EVM to reduce the overall gain, increase the IIP3, and improve the return loss (S11) of the EVM, but does result in an increase in the total noise figure. The gain is set such that saturation does not occur for a target at the closest range of 500 m. The two transformers provide single-ended to differential conversion with a good differential balance. The transformers on the ADC32RF45 EVM were replaced with Mini-Circuits TC1-1-43A+ because these transformers perform better at the receiver operating frequencies. The attenuator shown at the input of the ADC acts as a model for the bandwidth rolloff at the operating frequencies and was inferred from the total receiver gain, but aligns well with bandwidth measurements.

The gains in the lineup are based on measurements, but align with the data found in the respective datasheets. The noise figures used in the calculations are from datasheets, except for lossy elements where the noise figure is equal to the loss.

4.7   Design Extensions

The following subsections describe a few extensions to this reference design.

4.7.1   Performance

The specifications for this reference design have been mainly designed around hardware that was readily available in the lab. Most real-world receivers require lower noise figures, around 2 dB or less. This performance is certainly achievable using this receiver architecture by properly choosing the front end LNA and total receiver gain. Figure 8 shows an example lineup that achieves a 2-dB noise figure. A lower noise figure in the first low noise amplifier (LNA) and a higher overall gain optimizes the receiver for a better noise figure. The second amplifier is a linear amplifier with an additional drive capability to directly drive the ADC32RF45 device.

G = 19 dB
NF = 1.0 dB
IIP3 = 21 dBm

G = 15 dB
NF = 2.0 dB
IIP3 = 45 dBm

G = –0.34 dB
NF = 0.34 dB

G = 0 dB
NF = 0 dB

G = –1.2 dB
NF = 1.2 dB

G = –1.85 dB
NF = 1.85 dB

G = 0 dB
NF = 25.6 dB
IIP3 = 29 dBm

Totals:
G = 30.61 dB
NF = 1.99 dB
IIP3 = 1.87 dBm

Copyright © 2016, Texas Instruments Incorporated
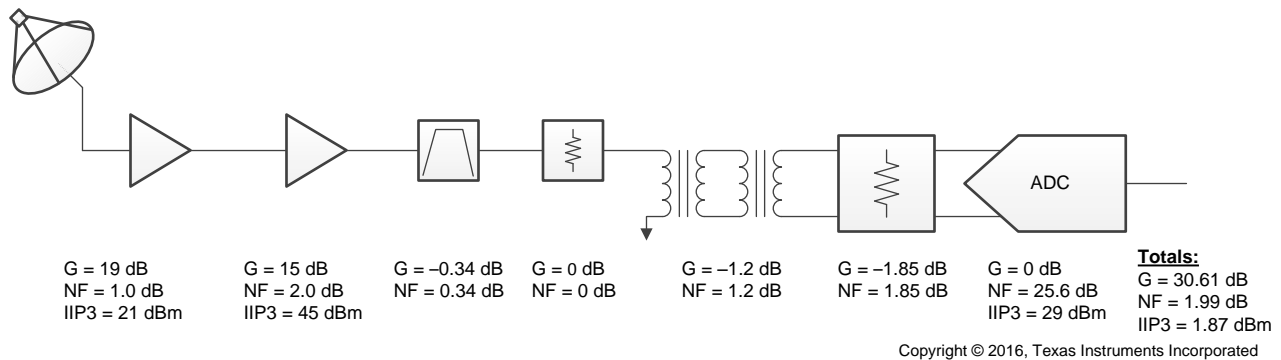
Figure 8. Example Lineup for 2-dB Receiver Noise Figure

4.7.2   Digital Downconverter

Bypassing the digital downconverter of the ADC32RF45 allows maximum, instantaneous frequency flexibility, which can be used for instances where systems require frequency hopping or maximum signal bandwidth. However, most systems do not require this degree of flexibility and system designers are likely to find that the use of the DDC reduces processing, power, and interface rate requirements.

As an example, the following **Figure 9** shows the external processing required in an FPGA or digital signal processor (DSP) to implement the detection algorithm. Note that Matlab software has been used to implement the quadrature-matched filter detector for the test data, which the following Figure 9 shows.

Decimating to a lower data rate is a desirable action to reduce the processing requirements for the matched filter implementation. Decimation by 8 has been used in this design to allow 300-MHz of signal BW, which is sufficient for the 100-MHz bandwidth LFM waveform.

Copyright © 2016, Texas Instruments Incorporated
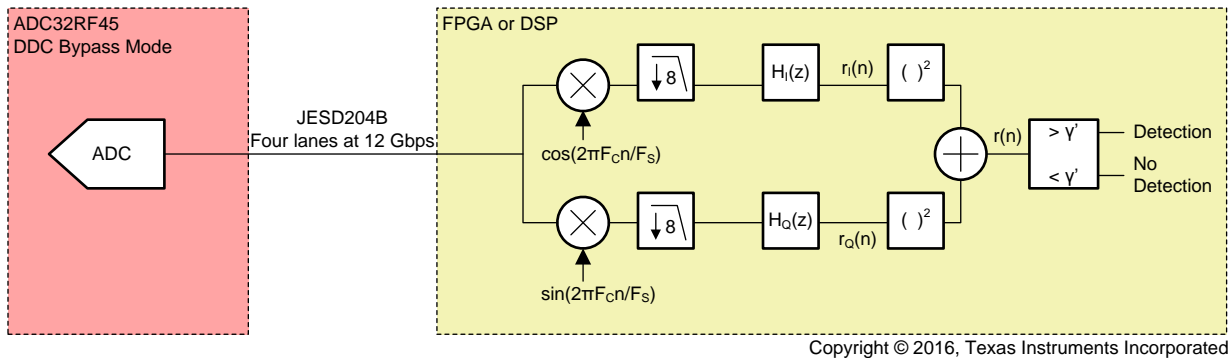
Figure 9. Detector Processing Block Diagram for ADC32RF45 in DDC Bypass Mode

An alternative approach to that shown in Figure 9 is to make use of the DDC inside of the ADC32RF45 device to off-load processing from the FPGA or DSP to reduce the resource requirements. Additionally, when using this alternative approach, the interface rate is significantly reduced. Instead of four serdes lanes at 12 Gbps, for a total throughput of 48 Gbps, the DDC enables reduction to two lanes at 7.5 Gbps, for a total throughput of 15 Gbps, which is a 68.75% reduction of the data rate and has an associated reduction in interface power consumption. The FPGA or DSP now just implements the quadrature-matched filter and detection rule (see Figure 10).
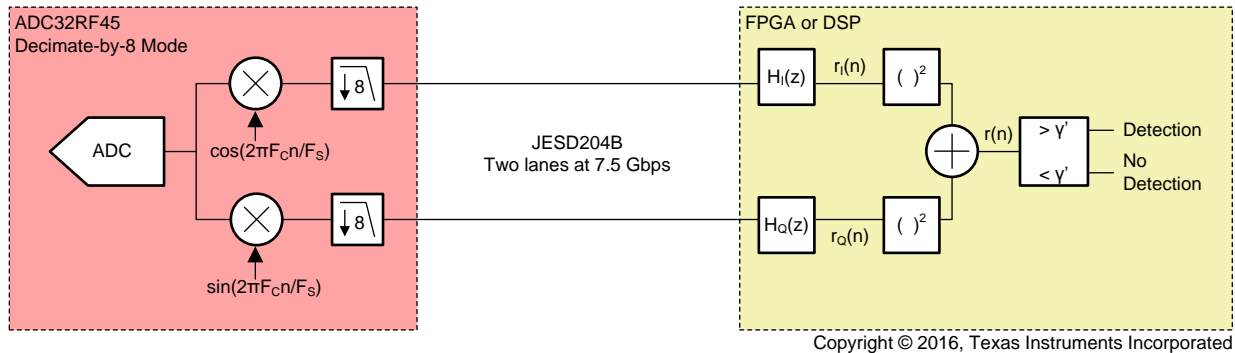
Figure 10. Detector Processing Block Diagram for ADC32RF45 in Decimate-by-8 Mode

The ADC32RF45 DDCs also have the ability to perform phase-coherent frequency hopping. Three numerically controlled oscillators (NCOs) are available per ADC channel. Each NCO can be set to a different operating frequency and run independently from the others. The desired frequency band is selected by choosing the appropriate NCO using the input pins of the device. The other NCOs continue to run to while a different NCO is selected to maintain the continuous phase.

5   Getting Started Hardware

5.1   ADC32RF45 EVM

See the ADC32RF45 EVM tool folder at http://www.ti.com/tool/adc32rf45evm.

5.2   TSW14J56 EVM

See the TSW14J56 EVM tool folder at http://www.ti.com/tool/tsw14j56evm.

6   Test Setup

Figure 11 shows a diagram of the test setup. The amplifiers, attenuator, and filters are components with SMA connectors for input and output connections and are external to the ADC32RF45 EVM.

The ADC32RF45 EVM connects to the TSW14J56 data capture card to capture the ADC output data. The data is downloaded to a computer for processing in Matlab. The ADC32RF45 EVM is set up such that the ADC receives its clock from an external clock source while the LMK04828 JESD204B-compliant clock jitter cleaner provides the SYSREF signals and other required clocks to the ADC and FPGA.
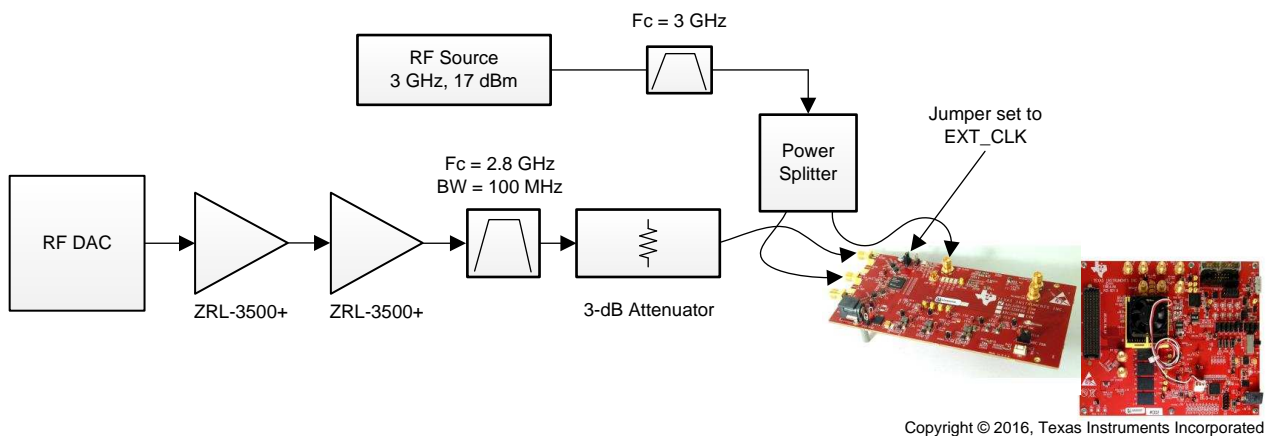
Figure 11. Lab Setup for Receiver Measurement and Verification

7   Test Data

This section contains a selection of measurements to verify performance and show application level results. Section 7.1 shows the gain and noise figure measurements. Section 7.2 shows the results of the matched filter output for simulated return signals.

7.1   *Gain and Noise Figure Verification*

The gain of the RF front end, from the input to the filter output, was measured using a network analyzer. Additionally, the filter was measured separately. The total gain was then measured using single tones placed across the band and by using the knowledge that the ADC32RF45 full-scale power is 6.59 dBm. The input power was measured using a spectrum analyzer before being applied to the receiver. Table 5 summarizes the results.

Table 5. Summary of Receiver Gain and Flatness

FREQUENCY (MHz)	INPUT POWER (dBm)	ADC OUTPUT POWER (dBFS)	ADC OUTPUT POWER (dBm)	GAIN (dB)	RIPPLE (dB)
2750	−62.95	−42.52	−35.93	27.02	0.53
2775	−63.16	−42.46	−35.87	27.29	0.8
2800	−63.1	−43.2	−36.61	26.49	0 (Reference)
2825	−62.88	−43.12	−36.53	26.35	−0.14
2850	−63.08	−43.96	−37.37	25.71	−0.78
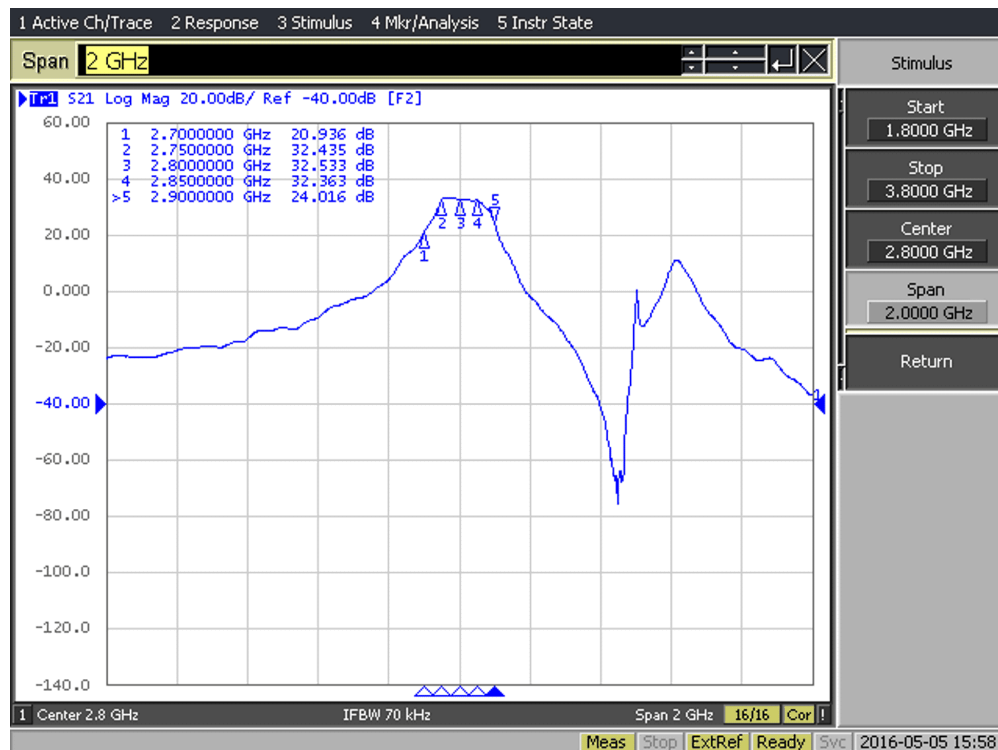
Figure 12. RF Front-End Gain Measurement (S21)
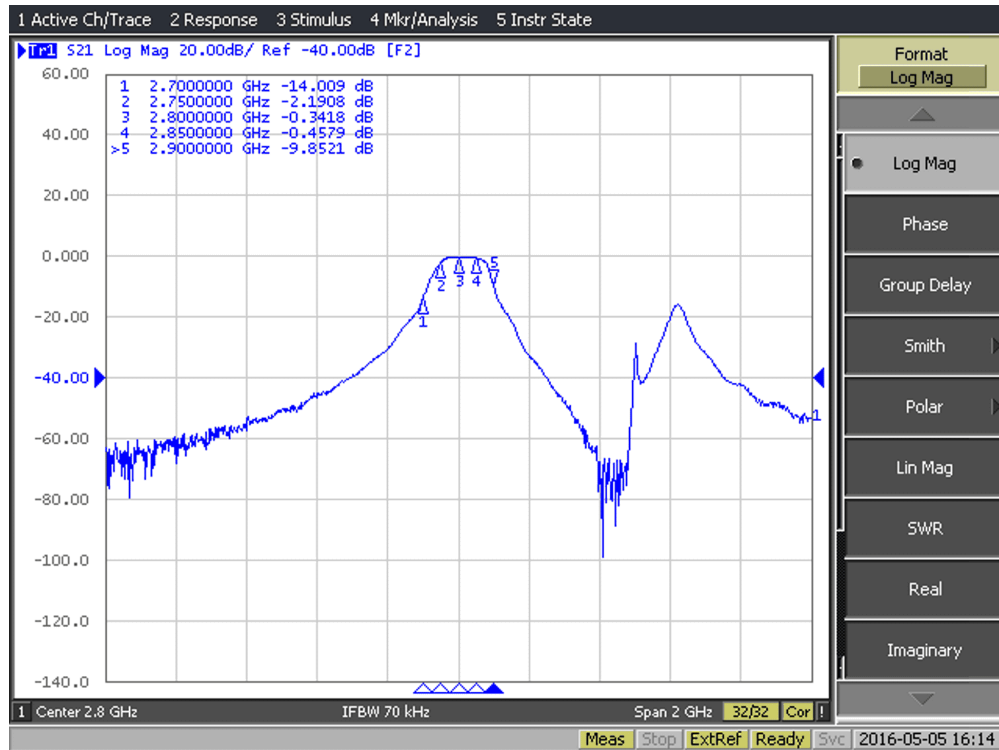
Figure 13. Filter Response Measurement (S21)

Determine the noise figure by measuring the noise of the receiver at the ADC output, subtracting the measured gain of the receiver, and finding the difference between the calculated input-referred noise and the thermal noise floor of –174 dBm/Hz. The plot in Figure 14 shows the output noise measurements and Table 6 shows the results and calculated noise figures. The noise figure measurements align well with the calculated noise figure of 4.53 dB. Figure 15 shows a measurement of the ADC noise floor with a terminated input for reference and is used to determine the noise figure of the ADC for the lineup analysis.
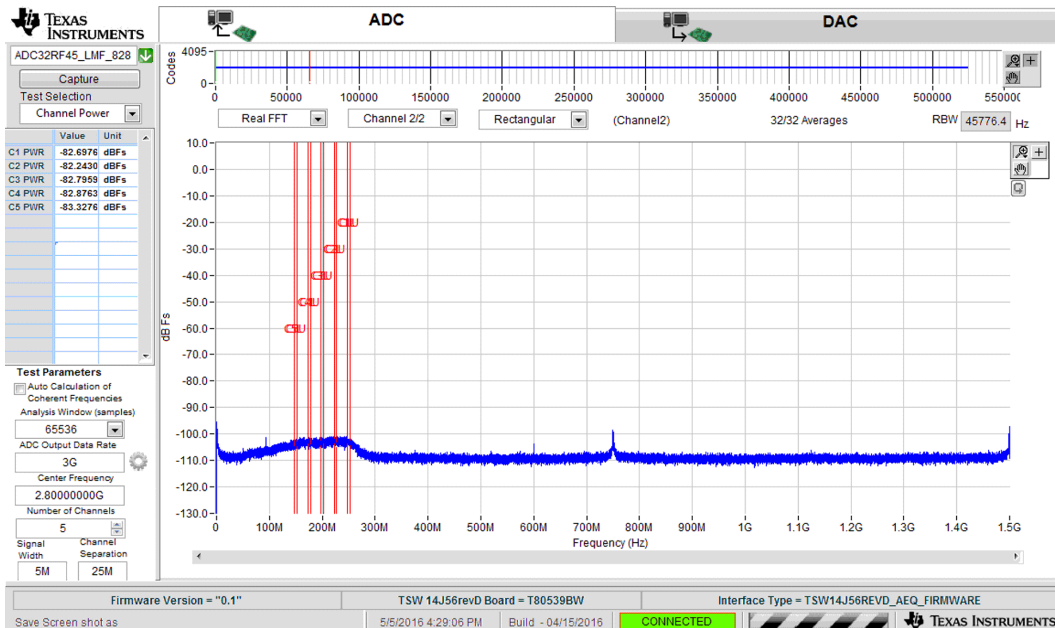
Figure 14. Receiver Noise Floor Measured at ADC Output
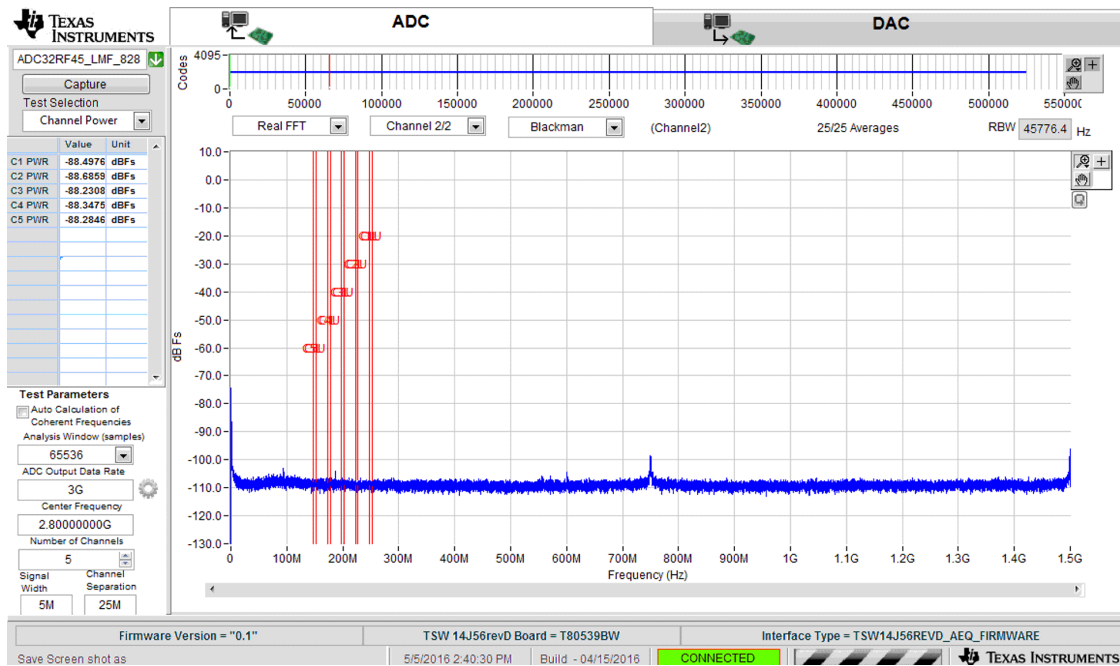
Figure 15. Noise Floor of 50-Ω Terminated ADC Without Receiver Front End

Table 6. Receiver Noise Measurements and Noise Figure Calculations

MEAS. FREQUENCY (MHz)	MEAS. BW (MHz)	MEAS. OUTPUT NOISE (dBFS)	MEAS. OUTPUT NOISE (dBFS/Hz)	MEAS. OUTPUT NOISE (dBm/Hz)	RX GAIN (dB)	INPUT REF. NOISE (dBm/Hz)	NOISE FIGURE (dB)
2750	5	−82.70	−149.69	−143.10	27.02	−170.12	3.88
2775	5	−82.24	−149.23	−142.64	27.29	−169.93	4.07
2800	5	−82.80	−149.79	−143.20	26.49	−169.69	4.31
2825	5	−82.88	−149.87	−143.28	26.35	−169.63	4.37
2850	5	−83.33	−150.32	−143.73	25.71	−169.44	4.56

7.2 *Calculation of Detection Threshold*

Determine the detection rule threshold, γ', by measuring the variance of the output of one of the matched filters, either $H_I(z)$ or $H_Q(z)$, when no signal is present. Figure 16 shows the output of the in-phase filter, $r_I(n)$, and gives the calculated variance of the matched filter output. Note that the variance is measured before the output is squared.
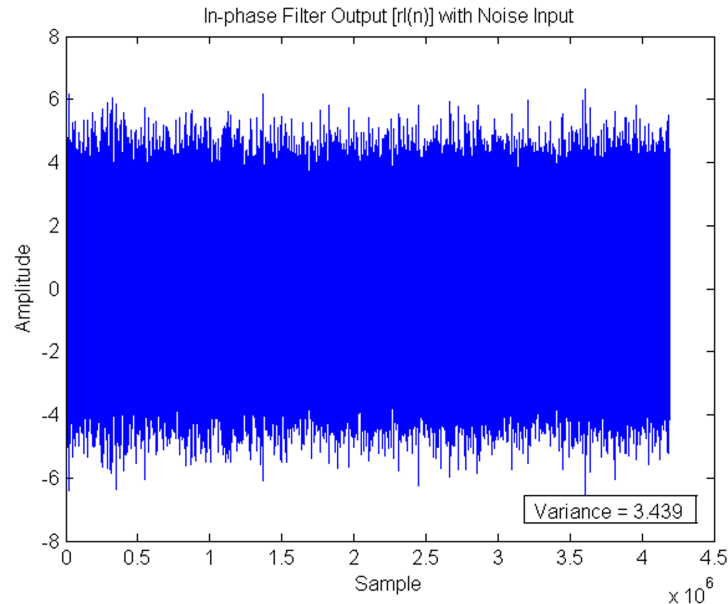
Figure 16. Matched Filter Output Noise for Detection Threshold Calculation

The P_{FA} equation (see preceding Equation 13) can then be used to solve for the appropriate threshold for a given noise variance, as the following Equation 18 shows. The detection probability has already been accounted for by determining the ENR from the look-up table.

$$\gamma' = -\sigma^2 \ln \times \left(P_{FA}\right) = -3.439 \ln \times \left(10^{-6}\right) = 47.5$$

(18)

7.3 *Radar Return Signal Measurements*

The radar return signals for the minimum and maximum ranges were created using a DAC to simulate a return signal, as shown in the following Figure 17, Figure 18, Figure 19, and Figure 20. The power of the return signals were calculated in Section 4.3. The signal in the figure is the output of the quadrature matched filter, r(n). Each figure has two peaks, the first is a reference peak that represents the pulse transmission and is not to scale. The second peak is the return signal at the expected return signal power. The red line represents the detection threshold. Table 7 and Table 8 summarize the results.
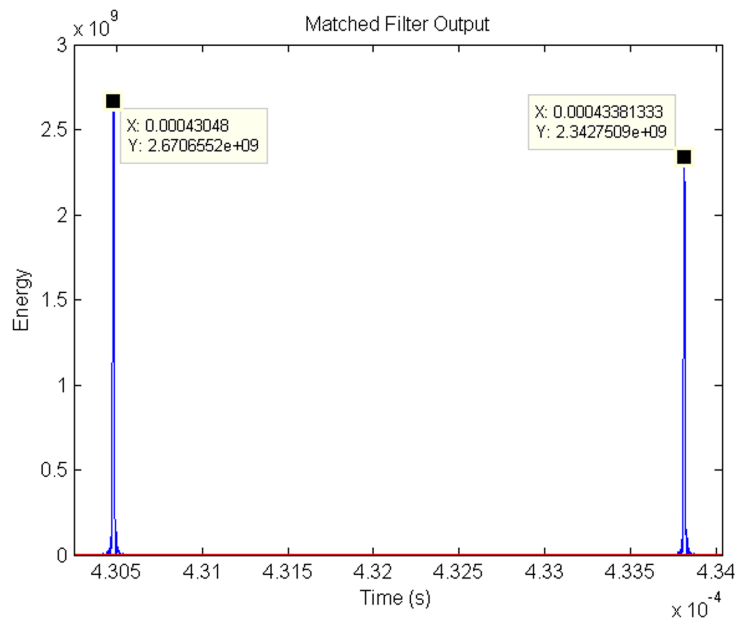
Figure 17. 500-m, 12.5-kW Transmit Power, 1-µs LFM Pulse
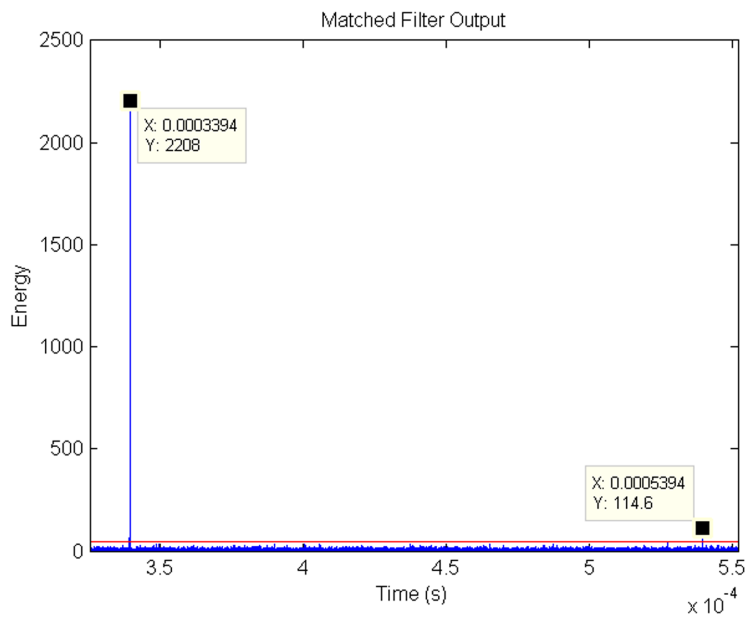
Figure 18. 30-km, 12.5-kW Transmit Power, 1-µs LFM Pulse
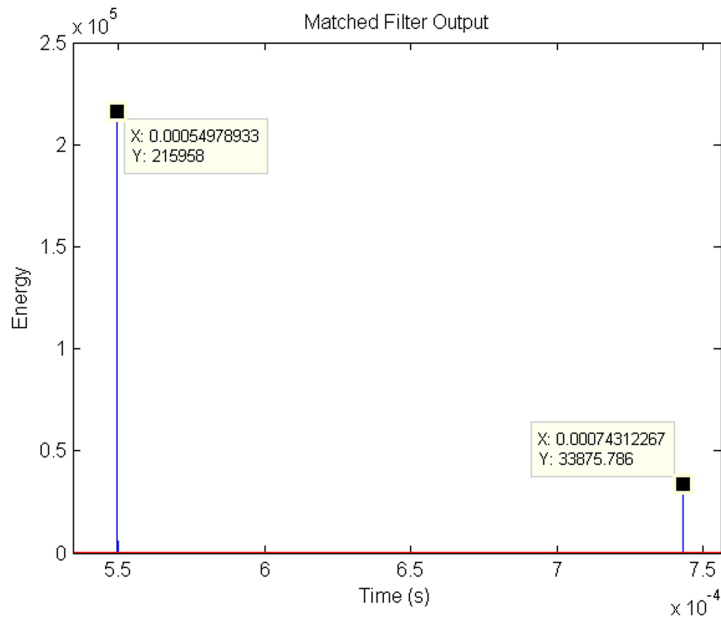
Figure 19. 29-km, 25-kW Transmit Power, 89-µs LFM Pulse
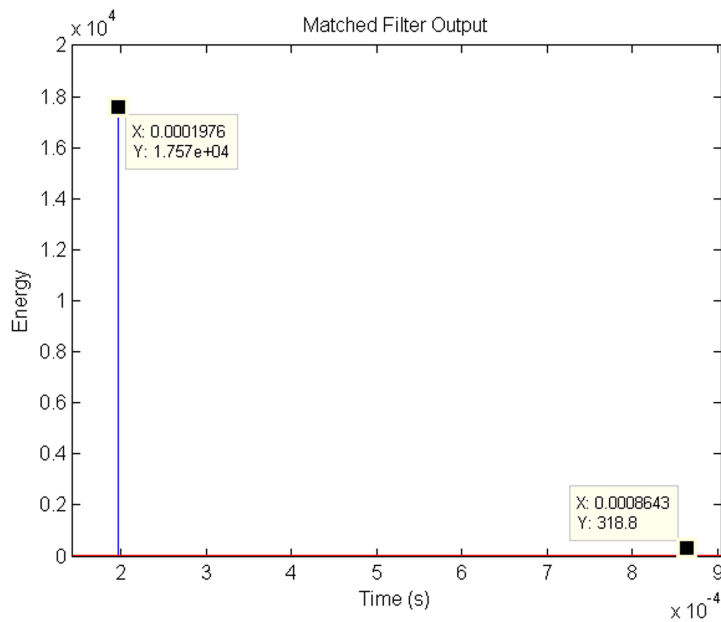
Figure 20. TIDUBS63051

Table 7. Summary of Return Time for Radar Return Signal Measurements

RANGE (km)	TRANSMIT POWER (kW)	PULSE LENGTH (µs)	REFERENCE TIME (µs)	RETURN TIME (µs)	MEASURED RETURN TIME (µs)	CALCULATED RANGE (km)
0.5	12.5	1	430.48	433.81333	3.33333	0.4999995
30	12.5	1	339.4	539.4	200.00	30.000
29	25	89	549.78933	743.12267	193.33334	29.000001
100	25	89	197.6	864.3	666.7	100.005

Table 8. Summary of Return Power for Radar Return Signal Measurements

RANGE (km)	TRANSMIT POWER (kW)	PULSE LENGTH (µs)	MATCHED FILTER OUTPUT r(n)	CALCULATED AMPLITUDE (LSBs)	CALCULATED RECEIVE POWER (dBm)	EXPECTED RECEIVE POWER (dBm)
0.5	12.5	1	2.3427509x109	1767.4	−21.18	−21.4
30	12.5	1	114.6	0.391	−94.29	−92.5
29	25	89	33875.786	0.712	−89.08	−88.9
100	25	89	318.8	0.069	−109.34	−110.4

Figure 21 shows a zoomed-in view of the return pulse from the 100-km measurement (from Figure 20). The pulse is narrow because of pulse compression from the long pulse length and the 100-MHz bandwidth LFM waveform. The narrow output pulse allows the radar to have better spatial resolution to detect nearby targets. The time-bandwidth product of the 89-µs pulse is 8900, whereas the time-bandwidth product of the 1-µs pulse is 100.
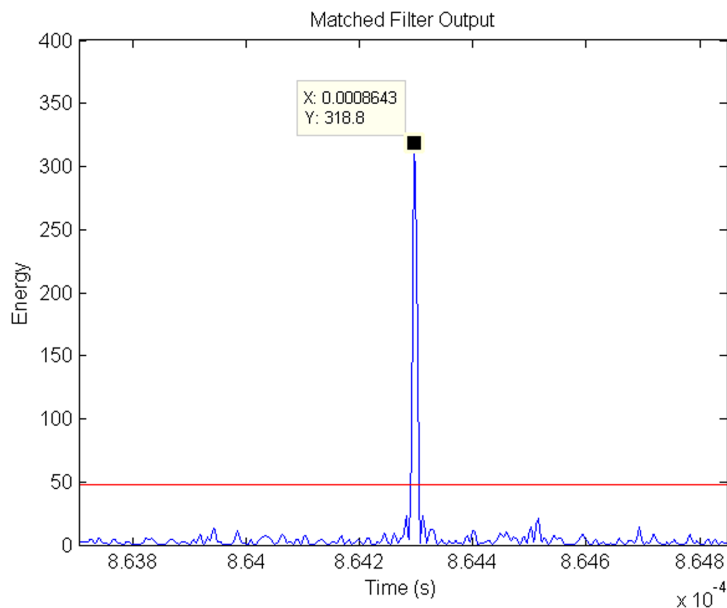
Figure 21. Return Signal From 100-km Return Measurement

8   Design Files

8.1   Schematics

To download the schematics, see the design files at TIDA-00814.

8.2   Bill of Materials

To download the bill of materials (BOM), see the design files at TIDA-00814.

8.3   Altium Project

To download the Altium project files, see the design files at TIDA-00814.

8.4   Gerber Files

To download the Gerber files, see the design files at TIDA-00814.

8.5   Assembly Drawings

To download the assembly drawings, see the design files at TIDA-00814.

9   Software Files

To download the software files, see the design files at TIDA-00814.

10   References

1. NTIA, *Analysis and Resolution of RF Interference to Radars Operating in the Band 2700-2900 MHz from Broadband Communication Transmitters*, NTIA Report TR-13-490, Oct 2012
2. U.S. Department of Transportation, *Airport Surveillance Radar Model 11 (ASR-11) FAA Test and Evaluation Master Plan (TEMP)*, U.S. Dept of Transportation Report DOT/FAA/CT-TN97/27, Feb 1998
3. Kay, Steven M.; *Fundamentals of Statistical Signal Processing, Volume II: Detection Theory*, 1st Ed; 1998
4. Skolnik, Merrill; *Radar Handbook*, 3rd Ed; 2008

11   About the Author

MATTHEW GUIBORD is a systems engineer in TI's high-speed data converters group. His focus is on aerospace and defense and test and measurement systems. Matt received his bachelor's degree from Michigan State University, East Lansing, Michigan.

IMPORTANT NOTICE FOR TI REFERENCE DESIGNS